RSC
Chemical Biology

ROYAL SOCIETY
OF **CHEMISTRY**

PAPER
Jean-Louis Reymond *et al.*
A mixed chirality α-helix in a stapled bicyclic and a linear
antimicrobial peptide revealed by X-ray crystallography

ROYAL SOCIETY OF CHEMISTRY

Check for updates

A mixed chirality α-helix in a stapled bicyclic and a linear antimicrobial peptide revealed by X-ray crystallography†

Stéphane Baeriswyl, [ID] ‡[a] Hippolyte Personne, [ID] ‡[a] Ivan Di Bonaventura, [ID][a] Thilo Köhler, [ID][b] Christian van Delden, [ID][b] Achim Stocker, [ID][a] Sacha Javor [ID][a] and Jean-Louis Reymond [ID] *[a]

The peptide α-helix is right-handed when containing amino acids with L-chirality, and left-handed with D-chirality, however mixed chirality peptides generally do not form α-helices unless a helix inducer such as the non-natural residue amino-isobutyric acid is used. Herein we report the first X-ray crystal structures of mixed chirality α-helices in short peptides comprising only natural residues as the example of a stapled bicyclic and a linear membrane disruptive amphiphilic antimicrobial peptide (AMP) containing seven L- and four D-residues, as complexes of fucosylated analogs with the bacterial lectin LecB. The mixed chirality α-helices are superimposable onto the homochiral α-helices and form under similar conditions as shown by CD spectra and MD simulations but non-hemolytic and resistant to proteolysis. The observation of a mixed chirality α-helix with only natural residues in the protein environment of LecB suggests a vast unexplored territory of α-helical mixed chirality sequences and their possible use for optimizing bioactive α-helical peptides.

Introduction

The primary amino acid sequence of a peptide or protein determines whether and which type of folded conformation it may form.[1] However, conformational preferences are almost exclusively documented and understood in the context of homochiral, all L- or all D-sequences, which form α-helices and β-sheets as canonical secondary structures. Studies with mixed chirality peptides have shown that they are generally not compatible with α-helical folding,[2–4] or form alternative secondary structures such as β-helices, α-strands, various types of β-turns, as well as intermolecular aggregates.[5–13] However, α-helical mixed chirality sequences have been directly observed by X-ray crystallography in peptides incorporating the non-natural residue amino-isobutyric acid as the α-helix inducer.[14–17] Incorporation of one or two D-residues in an α-helical L-peptide sometimes preserves helicity, as recently documented by X-ray crystallography for a macrocyclic peptide inhibitor of the p53–MDM2 interaction,[18] and by CD-spectroscopy in a stapled bicyclic peptide inhibitor of the EGF–EGFR complex[19] and a stapled peptide

KRAS inhibitor.[20] Note that mixed chirality 10/12 helices have been reported for β-peptides.[21]

In the case of antimicrobial peptides (AMPs), which are considered as an opportunity to address the public health threat of ESKAPE pathogens due to their ability to kill multidrug-resistant bacteria,[22–26] studies on short amphiphilic α-helical sequences have shown that mixed chirality analogs lose the ability to form α-helices, but often retain their antimicrobial activity while hemolysis and protease sensitivity are reduced.[27–31] In these studies, the deconvolution of relatively broad Fourier-transform infrared (FTIR) spectroscopy bands in the amide region suggested that some of the mixed chirality AMPs adopted random coil/α-helix/3₁₀-helix secondary structures in the membrane environment.[32–35] On the other hand, a recent atomic force microscopy study with random heterochiral AMP sequences in supported lipid bilayers suggested that these random AMPs do not fold, which would be compatible with a "carpet" type mechanism of membrane disruption suitable for the bactericidal effect, but not with pore formation required for hemolysis.[36] Our own recent studies with stereorandomized AMPs showed that the ensemble of all possible mixed chirality versions of α-helical AMPs do not have antibacterial or membrane disruptive activity, suggesting that amphiphilic folding is not possible with most mixed chirality sequences.[37]

In the context of developing AMPs with branched topologies against multi-drug resistant Gram-negative bacteria,[38–40] we

[a] *Department of Chemistry, Biochemistry and Pharmaceutical Sciences, University of Bern, Freiestrasse 3, 3012 Bern, Switzerland. E-mail: jean-louis.reymond@unibe.ch*
[b] *Department of Microbiology and Molecular Medicine, University of Geneva, Service of Infectious Diseases, University Hospital of Geneva, Geneva, Switzerland*
† Electronic supplementary information (ESI) available. See DOI: 10.1039/d1cb00124h
‡ Equal contributions.
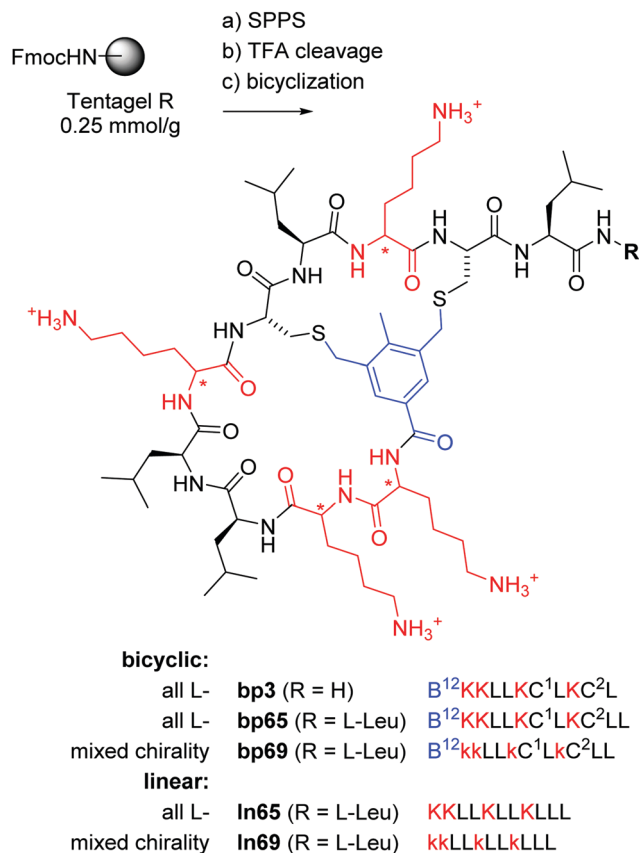
Fig. 1 Synthesis and structure of homochiral and mixed chirality AMBPs **bp3**, **bp65**, **bp69**, and the linear AMPs **ln65** and **ln69**. Conditions: (a) solid-phase peptide synthesis: (i) piperidine/DMF 1:4, 2 × 20 min, 50 °C, (ii) FmocAAOH (last coupling for bicyclic: 3,5-bis(chloromethyl)-4-methylbenzoic acid), DIC/oxyma, DMF, 50 °C; (b) TFA/TIS/DODT/H_2O 94:2.5:2.5:1, v/v/v/v, 3 h; (c) for bicyclic: H_2O/MeCN (50:50, v/v), KI (1 eq.), DIEA (5 eq.), 1 h. The line notation for bicyclic structures uses single letter codes for amino acids and the SMILES convention for cyclization points,[49,50] B = 3,5-bis(methylene)-toluoyl. All products were purified by preparative RP-HPLC.

recently identified antimicrobial bicyclic peptides (AMBPs) showing potent membrane disruptive and antibacterial activities.[41,42] However, all our AMBPs contained substantial acyclic portions and eluded precise structure determination. Capitalizing on our previous success in determining the structure of short peptides and peptide dendrimers by X-ray crystallography of lectin complexes,[43–48] we set out to obtain a direct structural insight into the bicyclic architecture of our AMBPs. Our starting point of choice was **bp3**, a weakly active but short AMBP prepared during a virtual screening guided campaign, in which all residues except its C-terminus resided within the loops (Fig. 1).[42]

Herein we report that optimization of **bp3** by sequence and residue chirality variations followed by structural studies led us to the first X-ray crystal structure of an AMPB in the form of **bp65**. The structure of **bp65** features an α-helical fold essentially identical to that of the corresponding linear peptide **ln65** but comprising a bicyclic helix staple. More importantly, our

study revealed the first X-ray crystal structure of mixed chirality α-helices with only natural amino acids in AMBP **bp69** containing seven L- and four D-residues and in the corresponding mixed chirality linear peptide **ln69**, both of which are almost perfectly superimposable with the homochiral α-helices of **bp65** and **ln65**.

Results and discussion

Optimizing a bicyclic antimicrobial peptide to a mixed chirality analog which retains activity as linear AMP

The previously identified AMBP **bp3** featured a particularly short sequence of only 10 residues, but was only active against the Gram-positive *Bacillus subtilis*, a bacterium which is particularly sensitive to membrane disruptive compounds.[42] An initial chemical space nearest neighbor search using molecular fingerprint similarity as described previously,[41,42] followed by synthesis and testing of eight close analogs of **bp3**, indicated that a second leucine residue at the C-terminus to form AMBP **bp65** increased the activity spectrum to *Pseudomonas aeruginosa* PAO1, our standard Gram-negative test strain, however at the cost of stronger hemolysis (**bp59–bp66**, Table S1, ESI† and Table 1).

To further optimize our AMBP, we prepared several diastereomers of **bp65**. While alternating L- and D-residues (**bp67**) produced an AMBP with both reduced hemolysis and reduced antibacterial activity, inverting only cysteines (**bp68**) or only lysines (**bp69**) preserved activity and hemolysis. To check whether cyclization was required for activity, we additionally prepared **ln65** and **ln69** as the linearized analogs of **bp65** and **bp69** by removing the N-terminal toluoyl staple and replacing both cysteines with leucines, as well as the corresponding **ln65b** and **ln69b** bearing an N-terminal toluoyl group and a pair of *S*-methyl cysteines corresponding more precisely to the composition of the bicyclic peptides. All four linear peptides showed antibacterial activities comparable to the parent bicyclic peptides, showing that cyclization was not required for activity (Table 1). Interestingly the two mixed chirality linear analogs **ln69** and **ln69b** additionally lost their hemolytic activity, an effect also sometimes observed with mixed chirality lysine/leucine containing AMPs.[28]

Vesicle leakage assays[51] showed that all peptides had substantial activity on anionic egg yolk phosphatidyl glycerol (EYPG) vesicles mimicking bacterial membranes. Furthermore, all compounds with hemolytic activity also induced leakage of zwitterionic egg yolk phosphatidyl choline (EYPC) vesicles mimicking eukaryotic membranes, the non-hemolytic peptides **bp67**, **ln69** and **ln69b** being the only compounds with very low leakage activity on these vesicles. These data suggested that our AMBP and their linear analogs acted by membrane disruption (Table 1 and Fig. S1, ESI†).

A closer characterization of AMBP **bp65** and **bp69** and their linear analogs **ln65**, **ln65b**, **ln69** and **ln69b** showed that these compounds had substantial activity against an extended panel of bacteria including multidrug-resistant strains (Table 2).

© 2021 The Author(s). Published by the Royal Society of Chemistry

RSC Chem. Biol., 2021, **2**, 1608–1617 | **1609**

Table 1 Synthesis and activity of bicyclic and linear AMPs

No.	Sequence[a]	SPPS yield[b] mg (%)	MS analysis calc./obs.[c]	MIC PAO1[d] (µg mL⁻¹)	Hemolysis on hRBC, MHC[e] (µg mL⁻¹)	EYPG vesicle leakage[f] (%)	EYPC vesicle leakage[f] (%)
bp3	B¹²KKLLKC¹ LKC²L	21.6 (15)	1330.81/1330.43	>64	500	—	—
bp65	B¹²KKLLKC¹LKC²LL	41.5 (26)	1443.89/1443.90	8	16.6	34	37
bp67	B¹²kKlLkC¹lKc²Ll	51.2 (33)	1443.89/1443.89	32	>2000	48	6
bp68	B¹²KKLLKc¹LKc²LL	55.7 (36)	1443.89/1443.79	16	16.6	44	18
bp69	B¹²kkLLkC¹LkC²LL	45.7 (29)	1443.89/1443.83	16	16.6	48	57
ln65	KKLLKLLKLLL	51.2 (33)	1320.99/1320.99	2–4	125	77	54
ln65b	TolKKLLKCₘLKCₘLL	84.0 (58)	1446.92/1446.92	4–8	16.6	40	49
ln69	kkLLkLLkLLL	45.7 (29)	1320.99/1320.99	8	1000	92	7
ln69b	TolkkLLkCₘLkCₘLL	102.6 (71)	1446.92/1446.92	16	1000	47	6

[a] One letter codes for amino acids, B = 3,5-bis(methylene)toluoyl, Tol = toluoyl group, Cₘ = S-methyl cysteine. Line notation for bicyclic structures uses single letter codes for amino acid and the SMILES convention for cyclization points.[49,50] [b] Yields given for RP-HPLC purified products. [c] High-resolution electrospray ionization mass spectrometry (positive mode), the calculated monoisotopic mass, and the observed mass in the reconstructed spectrum are given. [d] Minimum inhibitory concentration (MIC) was determined on *P. aeruginosa* PAO1 after incubation for 16–20 h at 37 °C. Values represent two independent triplicate MIC determinations. [e] Minimum hemolytic concentration (MHC) measured on human red blood cells in 10 mM phosphate buffer, 150 mM NaCl, pH 7.4, 25 °C. [f] Lipid vesicles made of EYPG or EYPC were suspended in buffer (10 mM TRIS, 107 mM NaCl, pH 7.4). After 45 s, the indicated compound was added to reach the indicated concentration. After 285 s, 30 µL of Triton X-100 1.2% was added for full fluorescein release. The percentage leakage observed with the 10 µg mL⁻¹ compound at 250 s is given. See Fig. S1 (ESI) for full curves.

Table 2 Extended activity profiling of bicyclic and linear AMPs

Cpd	*P. aeruginosa* ZEM-1A[a]	*P. aeruginosa* ZEM9A[a]	*K. pneumoniae* Oxa-48[a]	*E. coli* W3110[a]	*A. baumannii* BAL225[a]	*S. aureus* Newman[a]	*S. aureus* COL[a]	Serum stability (%)[b]
bp65	8	>32	16	8	4	8	8	93
bp69	4–8	>32	16	8	4	2–4	4	93
ln65	2–4	16	4	4	2–4	2–4	4	0
ln69	8	>32	8	4	2–4	8	16	96
ln65b	4	16	8	8	4	4	4	20
ln69b	8	>32	>32	8	8	32	32	96

[a] Minimal inhibitory concentration (MIC) in µg mL⁻¹ in the Mueller–Hinton (MH) broth after incubation for 16–20 h at 37 °C. [b] % of undegraded peptide after incubation in 25% human serum after 24 h. All experiments were performed in two independent triplicates. See Fig. S2 (ESI) for full curves.

While AMBPs **bp65** and **bp69** were both resistant to serum proteolysis as shown previously with other bicyclic peptides,[42,50] the linearized homochiral analogs **ln65** and **ln65b** were rapidly degraded (Table 2 and Fig. S2, ESI†). The mixed chirality linear AMPs **ln69** and **ln69b** however were entirely stable to serum proteolysis, similar to other mixed chirality AMPs,[27–31] random peptide mixtures[52,53] and stereo-randomized peptides.[37]

CD spectra indicate α-helical folding in a membrane environment

A helix-wheel analysis of AMBP **bp65** showed that its N-terminus and both cysteine residues resided on the same face of a possibly typical AMP-like amphiphilic α-helix with cationic and hydrophobic side chains on opposite sides of the helix (Fig. 2a). Indeed, **bp65** showed a CD (circular dichroism) spectrum typical for an α-helical AMP, with a transition from an unordered conformation in water to an α-helical conformation upon addition of up to 20% v/v trifluoroethanol (TFE) or in the presence of 5 mM n-dodecylphosphocholine (DPC) micelles mimicking the membrane environment (Fig. 2c). Its linear analogs **ln65** and **ln65b**, which had the same helix-wheel amphiphilic arrangement as **bp65** (Fig. 2b), showed similar

medium dependent CD spectra (Fig. 2d and Fig. S3, Table S2, ESI†), showing that, in contrast to hydrocarbon and related staples which most often increase α-helicity,[54–57] our bicyclic staple did not influence α-helical folding.

Surprisingly, the mixed chirality sequences **bp69** and **ln69** showed similar CD spectra and an even stronger α-helical signal as their homochiral parents in 5 mM DPC although they contained 7 L- and 4 D-residues (Fig. 2e, f and Fig. S3, Table S2, ESI†). These data suggested a membrane-induced helical folding reminiscent of the helical fold deduced on the basis of FTIR for certain mixed chirality AMPs.[32–35] In this case however, the linear peptide **ln69b** containing the N-terminal toluoyl group and a pair of S-methyl cysteines exactly matching **bp69** showed lower α-helicity in 20% TFE than **bp69** and **ln69**, suggesting a slightly lower folding ability (Table S2, ESI†), consistent with its lower antimicrobial and membrane disruptive activity (Tables 1 and 2).

X-ray crystallography shows α-helices in bicyclic, linear and mixed chirality AMPs

To get a direct insight into the structure of AMBP **bp65**/**bp69** and their linear analogs **ln65**/**ln69**, we performed several crystallization studies using either the compounds themselves
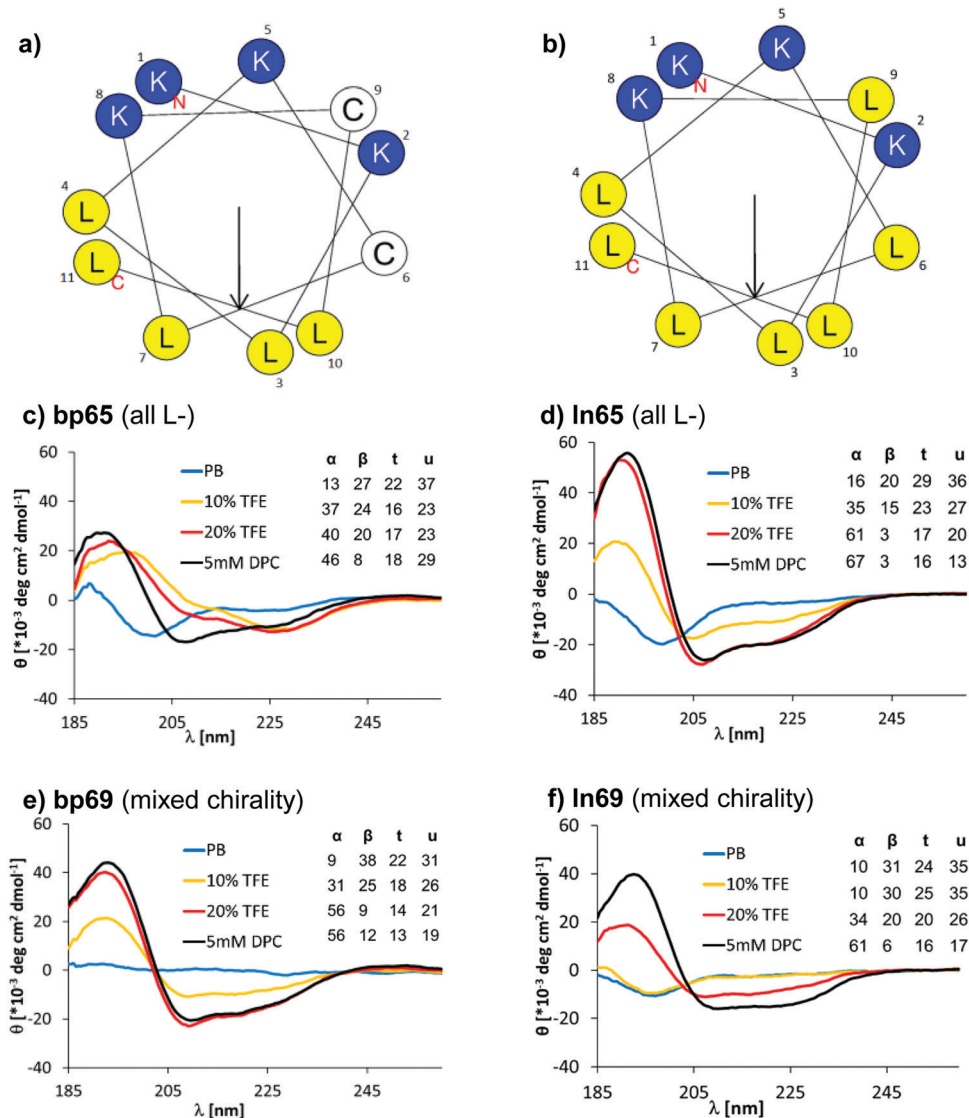
Fig. 2 (a) Helix properties of **bp65** predicted by HeliQuest.[58] Blue indicates cationic residues, yellow indicates hydrophobic residues and white indicates cysteines bound to the linker. The arrow inside the helix wheel indicates the magnitude and direction of the hydrophobic moment. (b) Same as (a) for **ln65**. (c) CD spectrum of **bp65** recorded at 0.100 mg mL^{-1} in 7 mM phosphate buffer at pH 7.2 with the addition of 0, 10, 20% TFE or 5 mM DPC. The primary CD spectra were analyzed using Dichroweb, and the percentages of secondary structures were extracted. α = alpha, β = beta, t = turn, u = unordered. The Contin-LL method and reference set 4 were used.[59] See the ESI† for full CD spectra (Fig. S3). (d) Same as (b) for **ln65**. (e) Same as (b) for **bp69**. (f) Same as (b) for **ln69**.

or their racemates to be crystallized as pure compounds, or their fucosylated derivatives of both mirror image peptides as complexes with the *P. aeruginosa* lectin LecB. From several hundred crystallization attempts under various conditions, we obtained seven well diffracting crystals (Table 3).

In the crystal structure of the homochiral AMBP **bp65** obtained as a racemic mixture with its D-enantiomer, the unit cell contained two non-equivalent peptides, each in L- and D-forms related by an inversion center (6Y14, 0.9 Å resolution, Table S3.1 and Fig. S4.1, ESI†). For the two structures obtained for **bp70**, an analog of **bp65** with multiple conservative exchanges of leucines and lysines, the unit cells were occupied by 6, respectively 24, symmetrically related copies of a single

peptide (PDB 6Y13, 1.1 Å resolution, Table S3.2 and Fig. S4.2, and PDB 6Y1S, 1.1 Å resolution, Table S3.3 and Fig. S4.3, ESI†). In all four individually resolved homochiral bicyclic structures, the peptides were present in almost perfectly superimposable conformations featuring nine of the eleven residues forming two full turns of a right-handed α-helix including the pair of stapling cysteines (Fig. 3A and B and Fig. S4.4, ESI†). The two N-terminal residues and the N-terminal toluoyl double staple formed a turn conformation. In all four cases the α-helical fold resulted in an amphiphilic arrangement of hydrophobic and cationic residues corresponding to the helix-wheel model and explaining the membrane disruptive activities discussed above (Fig. 3B).

Table 3 X-Ray crystallography of homochiral and mixed chirality AMBP and AMPs

No.	Sequence[a]	Conditions	PDB code	Res.	N^b
rac-**bp65**	B^{12}KKLLKC^{1}LKC^{2}LL/B^{12}kkllkc^{1}lkc^{2}ll	10 mg mL^{-1} peptide, 0.1 M sodium citrate pH 5.6, 35% v/v *t*-BuOH (crystal screen F5)	6Y14	0.9 Å	2
bp70	B^{12}HONleYDabC^{1}IRC^{2}YA	10 mg mL^{-1} peptide, 1.6 M (NH$_4$)$_2$SO$_4$, 0.1 M MES pH 6.5, 10% v/v 1,4-dioxane, 2% v/v glycerol (crystal screen F11 + 2% v/v Glycerol)	6Y13	1.1 Å	1
		10 mg mL^{-1} peptide, 0.2 M CaCl$_2$, 0.1 M NaOAc pH 4.6, 20% v/v i-PrOH (crystal screen B12)	6Y1S	1.1 Å	1
bp71	B^{12}kkLLkC^{1}LkC^{2}LLK(*)	40 µM LecB, 200 µM peptide, 1.5 M (NH$_4$)$_2$SO$_4$, 0.1 M Tris pH 8.5, 12% v/v glycerol (crystal screen H6)	6Y0U	1.5 Å	3
		40 µM LecB, 200 µM peptide, 0.01 M CoCl$_2$, 0.1 M NaOAc pH 4.6, 1.0 M 1,6-hexanediol (crystal screen E11)	6Y0V	1.7 Å	3
Fln65	(*)KKLLKLLKLLL	40 µM LecB, 200 µM peptide, 0.2 M magnesium formate dihydrate (crystal screen D8)	7NEF	1.5 Å	8
Fdln69	(*)KKllKllKlll	40 µM LecB, 200 µM peptide, 0.2 M sodium citrate, 0.1 M sodium cacodylate pH 6.5, 30% v/v i-ProH (crystal screen A8)	7NEW	2.0 Å	2

[a] One letter codes for amino acids, B = 3,5-bis(methylene)toluoyl, Nle = norleucine, Dab = diaminobutyric acid, * = α-L-fucosyl-acetyl. The line notation for bicyclic structures uses single letter codes for amino acids and the SMILES convention for cyclization points. The structural formulae of all compounds are shown in the ESI. [b] N = number of crystallographically non-equivalent structures.

For the mixed chirality AMBP **bp69**, we obtained two crystal structures of lectin LecB complexed with **bp71**, an analog of the mixed chirality AMBP **bp69** with an additional side-chain fucosylated lysine at the C-terminus. In these two very similar X-ray structures, three of the four non-equivalent fucose binding pockets were occupied by moderately to well resolved peptides in an α-helical conformation (PDB 6Y0U, 1.5 Å resolution, Table S3.4 and Fig. S4.5; and PDB 6Y0V, 1.7 Å resolution, Table S3.5 and Fig. S4.6, ESI†).[44,46–48] The remaining binding pocket showed electron densities only for the anchoring fucose, indicating a disordered conformation. The six individual structures of the mixed chirality AMBP featured essentially the same double-stapled amphiphilic α-helix as that observed in the parent homochiral AMBP structures (Fig. 3A and B).

In the case of the linear AMPs, we obtained X-ray crystal structures of the homochiral AMP **ln65** in the form of LecB complexes with the N-terminally fucosylated analog **Fln65** (PDB 7NEF, 1.51 Å resolution, Table S3.6 and Fig. S4.7, ESI†). The LecB complex with the homochiral sequence **Fln65** showed eight crystallographically distinct structures, which represented amphiphilic α-helices (Fig. 3A and B). Similarly, we obtained an X-ray crystal structure of the mixed chirality linear AMP **ln69** as a LecB complex of its N-terminally fucosylated enantiomer **Fdln69** (PDB 7NEW, 2.02 Å resolution, Table S3.7 and Fig. S4.8, ESI†). This structure contained four crystallographically non-equivalent fucose binding sites, two of which featured the peptide in a fully formed α-helix (Fig. 3A and B). The other pair of fucose binding sites only showed electron density for the anchoring fucosyl group and the first residue, indicating a disordered conformation, a situation also observed previously with other homochiral peptides and probably caused by crystal packing (Fig. S4.8, ESI†).[47]

Remarkably, the ten crystallographically non-equivalent stapled bicyclic α-helices observed in the X-ray structures of the homochiral *rac*-**bp65** and **bp70**, and the mixed chirality

bp71·LecB complex were essentially superimposable, with RMSD < 0.6 Å for the peptide backbones (Fig. 3C, left panel). The same was true across the ten different X-ray structures of linear α-helices observed in the X-ray structures of LecB complexes for the homochiral **Fln65** and its mixed chirality analog **Fdln69** (RMSD < 0.9 Å, Fig. 3C, right panel). This comparison showed that the helical geometries of the homochiral and heterochiral helices were not significantly different from each other.

Molecular dynamics simulations confirm the stability of homochiral and heterochiral α-helices in micelles or as helix bundles

While CD spectra indicated that in solution the different peptides were unordered in water and only folded in the presence of DPC micelles or with TFE mimicking the membrane environment, the X-ray structures presented above featured α-helices within the crystal environment in the absence of any membrane lipids. To better understand in which context the folded conformations were stable, we performed MD simulations using GROMACS.[60]

For the homochiral AMBP **bp65**, MD simulation in pure water resulted in rapid unfolding of the α-helix and formation of a disordered conformation. In the presence of a DPC micelle by contrast, the AMBP rapidly adsorbed to the micelle surface and refolded into an α-helix, reproducing the CD observation in the presence of micelles (Fig. 4a). MD simulations with the mixed chirality AMBP **bp69** gave similar results (Fig. 4b). To test whether the α-helix was stabilized by the bicyclic staple, we repeated the MD simulation with linear analogs **ln65** and **ln69**, which again showed rapid unfolding in water but refolding to a stable α-helix at the DPC micelle surface for both the homochiral linear peptide **ln65** and the mixed chirality linear peptide **ln69** (Fig. 4c and d). These simulations confirmed the similar folding behavior of homochiral and mixed chirality bicyclic or
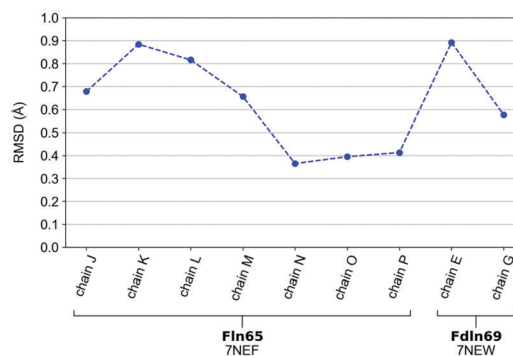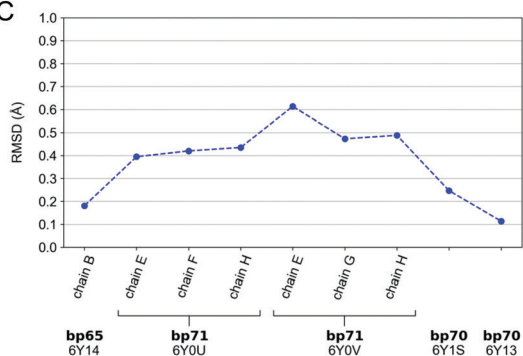
A

i) bp65 racemate
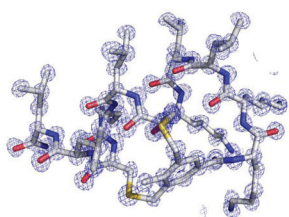
iii) Fln65·LecB complex (all L-)
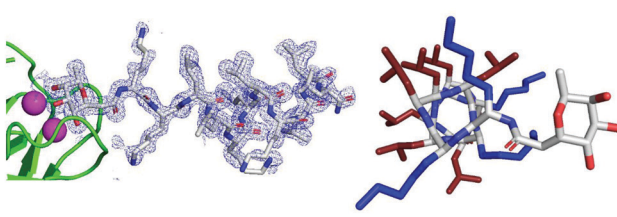
ii) bp71·LecB complex (mixed chirality)
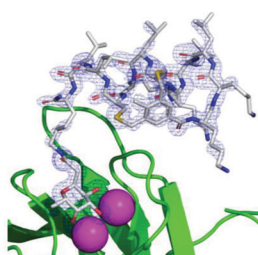
iv) FdIn69·LecB complex (mixed chirality)
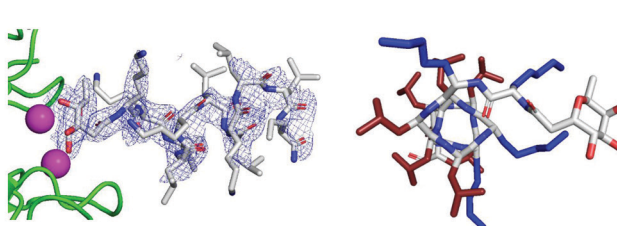
B

i) bp65 (all L-)
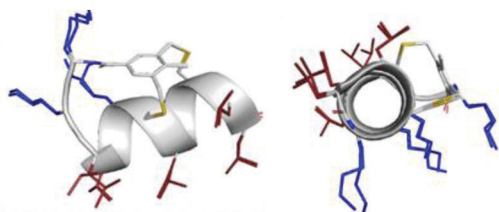
iii) Fln65 (all L-)
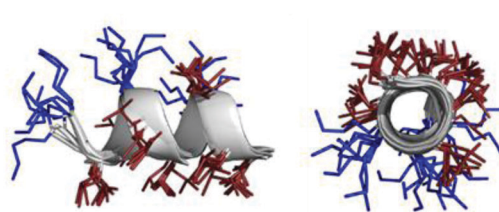
ii) bp71 (mixed chirality)
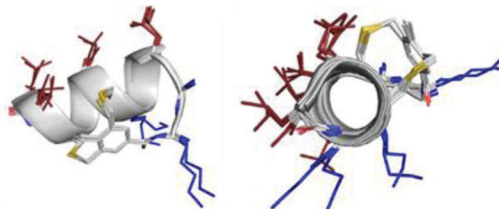
iv) FdIn69 (mixed chirality)
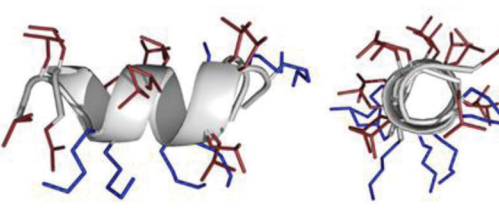
C

Fig. 3   (A) X-Ray crystallography of α-helical homochiral and mixed chirality AMPs and AMBPs. (i) X-Ray crystal structure of **bp65**. Left panel: Electron density as blue mesh corresponding to **bp65** observed in the X-ray crystal structure of the **bp65** racemate in PDB 6Y14. Right panel: Stick model of the **bp65** crystal structure, lysine side chains shown in blue and leucine side chains shown in brown. See the ESI† for details. (ii) X-Ray crystal structure of the **bp71**·LecB complex. Left panel: Electron density as blue mesh for **bp71** in one of the 4 crystallographically distinct LecB binding sites in PDB 6Y0U. Peptide, Ca^{2+} atoms and LecB monomer are represented as in (ii). Right panel: Stick model of **bp71** as observed in the crystal, with full side chains added for clarity, color coded as in (i). See the ESI† for details. (iii) X-Ray crystal structure of the **Fln65**·LecB complex. Left panel: Electron density (blue mesh) for

© 2021 The Author(s). Published by the Royal Society of Chemistry

RSC Chem. Biol., 2021, **2**, 1608–1617 | **1613**

Fln65 in one of the eight crystallographically distinct LecB binding sites in PDB 7NEF. The peptide is represented with s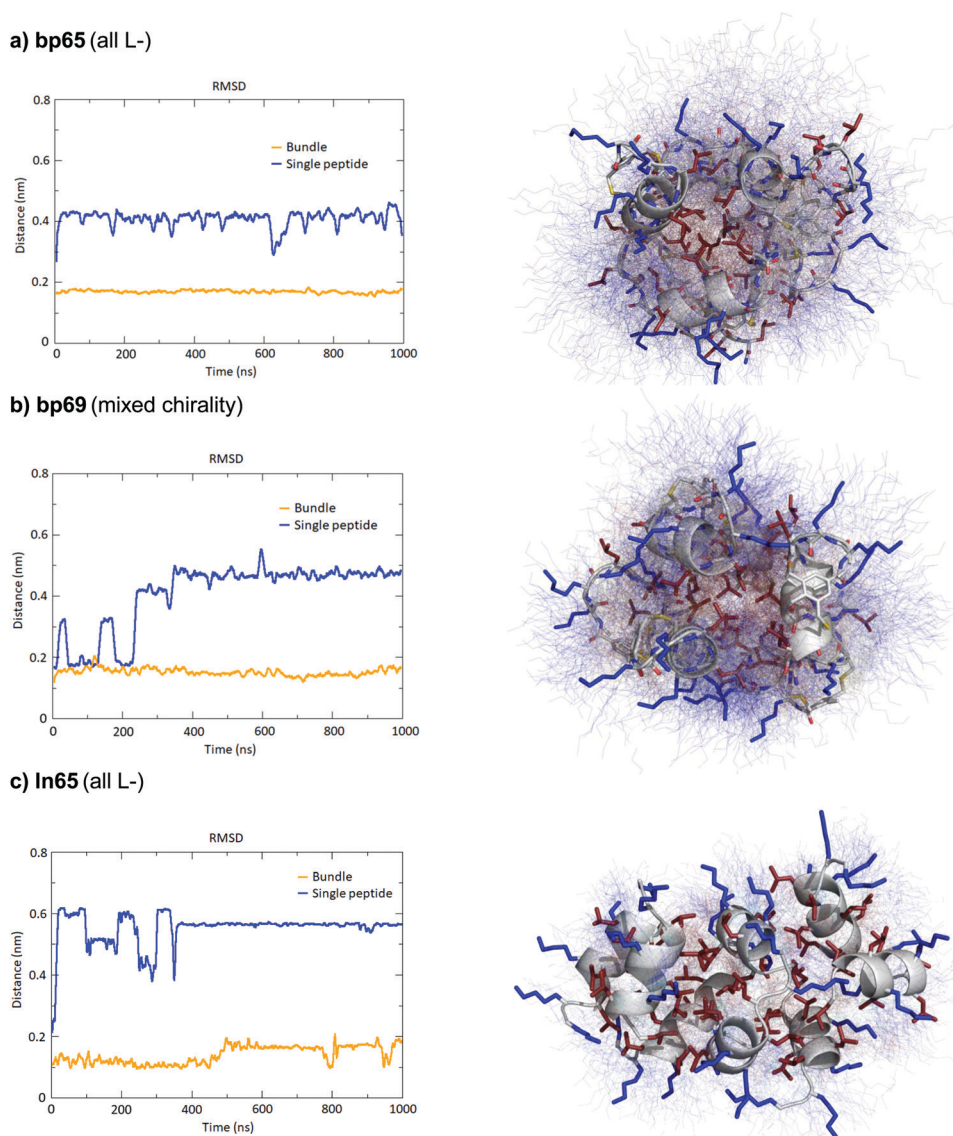ticks, Ca^{2+} atoms of the lectin binding site are shown with magenta spheres and the LecB monomer with green cartoon. Right panel: Stick model of **Fln65** as observed in the crystal structure, color coded as in (i). See the ESI† for details. (iv) X-Ray structure of the **Fdln69**·LecB complex. Left panel: Electron density (blue mesh) for **Fdln69** in one of the four crystallographically distinct LecB binding sites in PDB 7NEW. Peptide, Ca^{2+} atoms and the LecB monomer are represented as in (ii). Right panel: Stick model of **Fdln69** as observed in the crystal structure, color coded as in (i). See the ESI† for details. (B) Superpositions of non-equivalent peptides within the X-ray structures. (i) **bp65**: Superposition of the 2 non-equivalent L-peptides in the unit cell of PDB 6Y14. (ii) **bp71**: Superposition of the 6 most complete peptides of PDB entries 6Y0U and 6Y0V. (iii) **Fln65**: Superposition of the 8 non-equivalent peptides of PDB 7NEF. (iv) **Fdln69**: superposition of the 2 non-equivalent of PDB 7NEW. Peptides are shown as grey cartoon with the side chains as sticks. Amino acid side chains are color-coded: brown = hydrophobic, blue = cationic. (C) Left panel: Root-mean-square deviation (RMSD) calculated with PyMol between the backbone of **bp65** (6Y14, chain A) and the backbone of every non-equivalent bicyclic peptides obtained by X-ray crystallography: **bp65** (6Y14, chain B), **bp71** (6Y0U, chains E, F and H; 6Y0V, chains E, G and H) and **bp70** (6Y1S and 6Y13). Right panel: RMSD calculated with PyMol between the backbone of **Fln65** (7NEF, chain I) and the backbone of every non-equivalent linear peptide obtained by X-Ray crystallography of **Fln65** (7NEF, chains J, K, L, M, N, O and P) and **Fdln69** (7NEW, chains E and G). Enantiomers of both **Fdln69** chains were used for these calculations. All fucosyl groups were removed for superpositions and RMSD calculations.
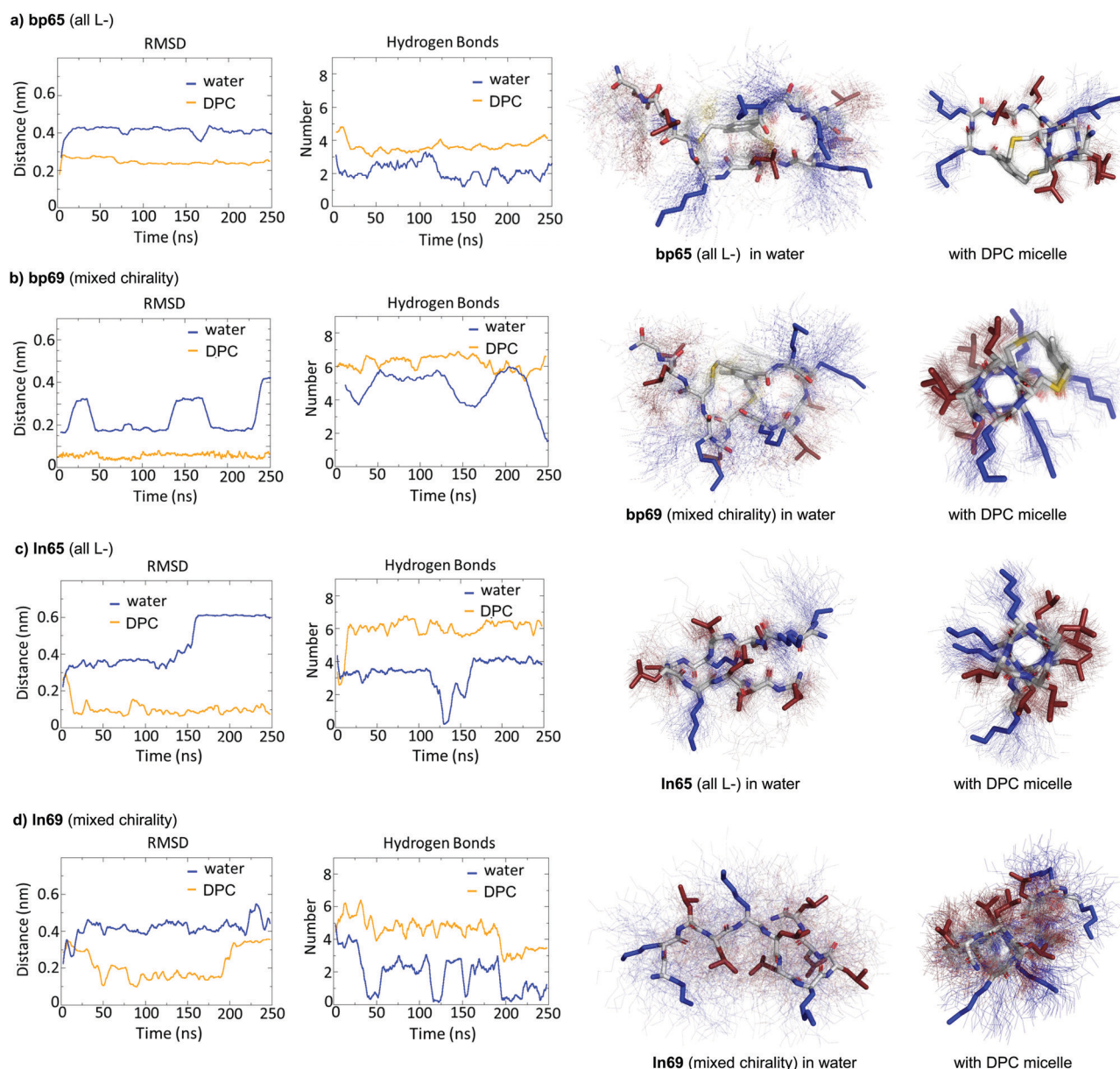
Fig. 4 MD simulations in water and in the presence of a DPC micelle. (a) MD simulation of **bp65** in water with/without a DPC micelle over 250 ns using GROMACS. Left panel: Root-mean-square deviation of the peptide backbone atoms relative to starting coordinates observed in the crystal structure of **bp65**. Center left panel: Number of intramolecular backbone hydrogen bonds. Center right and right panels: Average structure (stick model) in water (center right) or with DPC micelle (right panel) over 100 structures sampled over the last 100 ns (thin lines). (b) Same as (a) for **bp69**, starting from the α-helical coordinates observed in the crystal structure of the LecB·**bp71** complex. (c) Same as (a) for **ln65** starting from the α-helix model built in PyMol. (d) Same as (a) for **ln69** starting from the α-helix model built in PyMol. The DPC micelle was omitted for clarity.

1614 | *RSC Chem. Biol.*, 2021, **2**, 1608–1617

© 2021 The Author(s). Published by the Royal Society of Chemistry

a) bp65 (all L-)

b) bp69 (mixed chirality)

c) ln65 (all L-)

Fig. 5 MD simulations of helix bundles for **bp65**, **bp69** and **ln65** from X-ray structures of **bp65**, **bp71** and **Fdln65**. (a) MD simulations of **bp65** as a bundle. Left panel: Root mean square distances of the backbone atoms relative to the backbone atoms of the starting model of a single peptide in the bundle compared to single peptides in water. Right panel: Overlay of 100 states over the 1000 ns run trajectory of the bundle in water. The average structure is shown as cartoon (backbone) and sticks (sidechains) and the 100 states as thin lines. Hydrophobic side chains are colored in red and cationic side chains in blue. (b) Same as (a) for **bp69** for the bundle containing three complete peptides in the bundle out of four. (c) Same as (a) for **ln65**. All fucoses were removed before simulations.

linear peptides, both requiring a membrane-like environment to form, and provided further evidence that the bicyclic staple did not contribute to helix stability.

The MD simulations in water and DPC micelles were consistent with the CD observations but did not explain why α-helices could be observed in the X-ray crystal structures where the peptides are surrounded only by a largely aqueous solvent. A closer analysis of the different X-ray structures showed that the peptides did not make any significant contact with LecB apart from the anchoring fucose residue. In the case of **bp65**, **bp71** and **Fln65** the peptides were aggregated in bundles of four of more helices *via* hydrophobic contacts between leucine side

chains. MD simulations showed that these helix bundles were stable in water and retained the α-helical fold of the individual peptides thanks to stabilizing hydrophobic contacts in the absence of a membrane environment as observed previously with related AMPs (Fig. 5 and Fig. S5, ESI†).[47]

Conclusions

By investigating the structure of AMPBs we discovered the mixed chirality sequence **bp69** containing seven L- and four D-residues folding into an amphiphilic α-helix within a stapled

© 2021 The Author(s). Published by the Royal Society of Chemistry

RSC Chem. Biol., 2021, **2**, 1608–1617 | **1615**

bicyclic peptide similar to the parent all L-AMBP **bp65**. A similar α-helical fold was observed for the corresponding linear mixed chirality peptide **ln69** and the homochiral sequence **ln65**. The mixed chirality linear AMP **ln69** showed comparably strong antibacterial activities but reduced hemolysis and much stronger stability against serum proteolysis compared to its homochiral parent **ln65**, similar to previous reports with mixed chirality AMPs.[27–35] The homochiral or heterochiral bicyclic and linear α-helices were observed by CD in a micellar environment as well as by X-ray crystallography of peptides or their complexes with LecB. MD simulations confirmed that the mixed chirality formed comparably well to the homochiral helices in micelles or as helix bundles in water as observed by X-ray crystallography.

While previous reports of similar mixed chirality AMPs concluded on either unordered conformations or helical conformations appearing in a membrane environment based on deconvolution of FTIR spectra,[32–35] here we reported X-ray crystallographic evidence of short mixed chirality helices consisting of only natural residues existing as helix bundles within the protein environment of a lectin and almost perfectly superimposable with their parent homochiral α-helices. These direct observations unequivocally demonstrate that the α-helical fold with only natural residues can sometimes tolerate multiple stereochemical inversions without significant conformational changes. Together with the fact that mixed chirality sequences appear to be entirely stable in serum, our observation suggests a vast unexplored territory of α-helical mixed chirality sequences as stabilized replacements for all L-bioactive α-helical peptides.

Methods

Synthesis and characterization of peptides and all assays, measurements, and modeling studies are described in the ESI.† No unexpected or unusually high safety hazards were encountered.

Author contributions

SB and HP designed and carried out structural and functional studies and modeling simulations and wrote the paper. IDB designed the study, and synthesized and characterized bicyclic peptides. TK and CvD designed and supervised experiments with MDR bacteria. AS supervised and carried out X-ray crystallography. SJ supervised molecular dynamics studies and wrote the paper. JLR designed and supervised the study and wrote the paper. All authors read and commented on the paper.

Conflicts of interest

The authors declare no competing financial interest.

Acknowledgements

References

1 A. W. Senior, R. Evans, J. Jumper, J. Kirkpatrick, L. Sifre, T. Green, C. Qin, A. Žídek, A. W. R. Nelson, A. Bridgland, H. Penedones, S. Petersen, K. Simonyan, S. Crossan, P. Kohli, D. T. Jones, D. Silver, K. Kavukcuoglu and D. Hassabis, *Nature*, 2020, **577**, 706–710.

2 V. Nanda and W. F. DeGrado, *J. Am. Chem. Soc.*, 2006, **128**, 809–816.

3 N. E. Shepherd, H. N. Hoang, G. Abbenante and D. P. Fairlie, *J. Am. Chem. Soc.*, 2009, **131**, 15877–15886.

4 C. Bleiholder, N. F. Dupuis, M. M. Gessel and M. T. Bowers, *Int. J. Mass Spectrom.*, 2017, **413**, 52–60.

5 B. M. Burkhart, N. Li, D. A. Langs, W. A. Pangborn and W. L. Duax, *Proc. Natl. Acad. Sci. U. S. A.*, 1998, **95**, 12950–12955.

6 S. Fernandez-Lopez, H. S. Kim, E. C. Choi, M. Delgado, J. R. Granja, A. Khasanov, K. Kraehenbuehl, G. Long, D. A. Weinberger, K. M. Wilcoxen and M. R. Ghadiri, *Nature*, 2001, **412**, 452–455.

7 E. Alexopoulos, A. Küsel, G. M. Sheldrick, U. Diederichsen and I. Usón, *Acta Crystallogr., Sect. D: Biol. Crystallogr.*, 2004, **60**, 1971–1980.

8 S. Durani, *Acc. Chem. Res.*, 2008, **41**, 1301–1308.

9 S. Basak, I. Singh, A. Ferranco, J. Syed and H.-B. Kraatz, *Angew. Chem., Int. Ed.*, 2017, **56**, 13288–13292.

10 T. M. Clover, C. L. O'Neill, R. Appavu, G. Lokhande, A. K. Gaharwar, A. E. Posey, M. A. White and J. S. Rudra, *J. Am. Chem. Soc.*, 2020, **142**, 19809–19813.

11 S. Kralj, O. Bellotto, E. Parisi, A. M. Garcia, D. Iglesias, S. Semeraro, C. Deganutti, P. D'Andrea, A. V. Vargiu, S. Geremia, R. De Zorzi and S. Marchesan, *ACS Nano*, 2020, **14**, 16951–16961.

12 V. K. Mulligan, C. S. Kang, M. R. Sawaya, S. Rettie, X. Li, I. Antselovich, T. W. Craven, A. M. Watkins, J. W. Labonte, F. DiMaio, T. O. Yeates and D. Baker, *Protein Sci.*, 2020, **29**, 2433–2445.

13 P. K. Hazam, C. Phukan, R. Akhil, A. Singh and V. Ramakrishnan, *Sci. Rep.*, 2021, **11**, 1823.

14 Y. Demizu, H. Yamashita, M. Doi, T. Misawa, M. Oba, M. Tanaka and M. Kurihara, *J. Org. Chem.*, 2015, **80**, 8597–8603.

15 Y. Demizu, H. Yamashita, T. Misawa, M. Doi, M. Oba, M. Tanaka and M. Kurihara, *Eur. J. Org. Chem.*, 2016, 840–846.

16 S. Aravinda, N. Shamala, S. Desiraju and P. Balaram, *Chem. Commun.*, 2002, 2454–2455.

17 I. L. Karle, H. N. Gopi and P. Balaram, *Proc. Natl. Acad. Sci. U. S. A.*, 2003, **100**, 13946–13951.

18 A. W. Partridge, H. Y. K. Kaan, Y.-C. Juang, A. Sadruddin, S. Lim, C. J. Brown, S. Ng, D. Thean, F. Ferrer, C. Johannes, T. Y. Yuen, S. Kannan, P. Aronica, Y. S. Tan, M. R. Pradhan, C. S. Verma, J. Hochman, S. Chen, H. Wan, S. Ha, B. Sherborne, D. P. Lane and T. K. Sawyer, *Molecules*, 2019, **24**, 2292.

19 S. Guardiola, J. Seco, M. Varese, M. Díaz-Lobo, J. García, M. Teixidó, L. Nevola and E. Giralt, *ChemBioChem*, 2018, **19**, 76–84.

20 L. Xu, C. Li, L. An, Z. Dai, X. Chen, Q. You, C. Hu and B. Di, *Eur. J. Med. Chem.*, 2020, **185**, 111844.

21 G. V. M. Sharma, K. R. Reddy, P. R. Krishna, A. R. Sankar, K. Narsimulu, S. K. Kumar, P. Jayaprakash, B. Jagannadh and A. C. Kunwar, *J. Am. Chem. Soc.*, 2003, **125**, 13670–13671.

22 L. T. Nguyen, E. F. Haney and H. J. Vogel, *Trends Biotechnol.*, 2011, **29**, 464–472.

23 B. Mojsoska and H. Jenssen, *Pharmaceuticals*, 2015, **8**, 366–415.

24 M. Magana, M. Pushpanathan, A. L. Santos, L. Leanse, M. Fernandez, A. Ioannidis, M. A. Giulianotti, Y. Apidianakis, S. Bradfute, A. L. Ferguson, A. Cherkasov, M. N. Seleem, C. Pinilla, C. de la Fuente-Nunez, T. Lazaridis, T. Dai, R. A. Houghten, R. E. W. Hancock and G. P. Tegos, *Lancet Infect. Dis.*, 2020, **20**, e216–e230.

25 N. Mookherjee, M. A. Anderson, H. P. Haagsman and D. J. Davidson, *Nat. Rev. Drug Discovery*, 2020, **19**, 311–332.

26 D. M. P. D. Oliveira, B. M. Forde, T. J. Kidd, P. N. A. Harris, M. A. Schembri, S. A. Beatson, D. L. Paterson and M. J. Walker, *Clin. Microbiol. Rev.*, 2020, **33**(3), e00181–19.

27 Y. Shai and Z. Oren, *J. Biol. Chem.*, 1996, **271**, 7305–7308.

28 Z. Oren, J. Hong and Y. Shai, *J. Biol. Chem.*, 1997, **272**, 14643–14649.

29 Y. Shai and Z. Oren, *Peptides*, 2001, **22**, 1629–1641.

30 U. Pag, M. Oedenkoven, N. Papo, Z. Oren, Y. Shai and H.-G. Sahl, *J. Antimicrob. Chemother.*, 2004, **53**, 230–239.

31 P. Wang, Y. H. Nan, S.-T. Yang, S. W. Kang, Y. Kim, I.-S. Park, K.-S. Hahm and S. Y. Shin, *Peptides*, 2010, **31**, 1251–1261.

32 J. Hong, Z. Oren and Y. Shai, *Biochemistry*, 1999, **38**, 16963–16973.

33 Z. Oren and Y. Shai, *Biochemistry*, 2000, **39**, 6103–6114.

34 N. Papo, Z. Oren, U. Pag, H.-G. Sahl and Y. Shai, *J. Biol. Chem.*, 2002, **277**, 33913–33921.

35 N. Papo and Y. Shai, *J. Biol. Chem.*, 2005, **280**, 10378–10387.

36 Z. Hayouka, A. Bella, T. Stern, S. Ray, H. Jiang, C. R. M. Grovenor and M. G. Ryadnov, *Angew. Chem., Int. Ed.*, 2017, **56**, 8099–8103.

37 T. N. Siriwardena, B.-H. Gan, T. Köhler, C. van Delden, S. Javor and J.-L. Reymond, *ACS Cent. Sci.*, 2021, **7**, 126–134.

38 M. Stach, T. N. Siriwardena, T. Kohler, C. van Delden, T. Darbre and J. L. Reymond, *Angew. Chem., Int. Ed.*, 2014, **53**, 12827–12831.

39 B.-H. Gan, T. N. Siriwardena, S. Javor, T. Darbre and J.-L. Reymond, *ACS Infect. Dis.*, 2019, **5**, 2164–2173.

40 B.-H. Gan, X. Cai, S. Javor, T. Köhler and J.-L. Reymond, *Molecules*, 2020, **25**, 5643.

41 I. Di Bonaventura, X. Jin, R. Visini, D. Probst, S. Javor, B. H. Gan, G. Michaud, A. Natalello, S. M. Doglia, T. Kohler, C. van Delden, A. Stocker, T. Darbre and J. L. Reymond, *Chem. Sci.*, 2017, **8**, 6784–6798.

42 I. Di Bonaventura, S. Baeriswyl, A. Capecchi, B.-H. Gan, X. Jin, T. N. Siriwardena, R. He, T. Kohler, A. Pompilio, G. Di Bonaventura, C. van Delden, S. Javor and J.-L. Reymond, *Chem. Commun.*, 2018, **54**, 5130–5133.

43 A. Imberty, M. wimmerova, E. P. Mitchell and N. Gilboa-Garber, *Microbes Infect.*, 2004, **6**, 221–228.

44 G. Michaud, R. Visini, M. Bergmann, G. Salerno, R. Bosco, E. Gillon, B. Richichi, C. Nativi, A. Imberty, A. Stocker, T. Darbre and J.-L. Reymond, *Chem. Sci.*, 2015, **7**, 166–182.

45 R. Visini, X. Jin, M. Bergmann, G. Michaud, F. Pertici, O. Fu, A. Pukin, T. R. Branson, D. M. Thies-Weesie, J. Kemmink, E. Gillon, A. Imberty, A. Stocker, T. Darbre, R. J. Pieters and J. L. Reymond, *ACS Chem. Biol.*, 2015, **10**, 2455–2462.

46 P. Roethlisberger, A. Istrate, M. J. Marcaida Lopez, R. Visini, A. Stocker, J. L. Reymond and C. J. Leumann, *Chem. Commun.*, 2016, **52**, 4749–4752.

47 S. Baeriswyl, B.-H. Gan, T. N. Siriwardena, R. Visini, M. Robadey, S. Javor, A. Stocker, T. Darbre and J.-L. Reymond, *ACS Chem. Biol.*, 2019, **14**, 758–766.

48 S. Baeriswyl, S. Javor, A. Stocker, T. Darbre and J.-L. Reymond, *Helv. Chim. Acta*, 2019, **102**, e1900178.

49 M. Bartoloni, R. U. Kadam, J. Schwartz, J. Furrer, T. Darbre and J.-L. Reymond, *Chem. Commun.*, 2011, **47**, 12634–12636.

50 M. Bartoloni, X. Jin, M. J. Marcaida, J. Banha, I. Dibonaventura, S. Bongoni, K. Bartho, O. Grabner, M. Sefkow, T. Darbre and J.-L. Reymond, *Chem. Sci.*, 2015, **6**, 5473–5490.

51 A. Hennig, G. J. Gabriel, G. N. Tew and S. Matile, *J. Am. Chem. Soc.*, 2008, **130**, 10338–10344.

52 Z. Hayouka, S. Chakraborty, R. Liu, M. D. Boersma, B. Weisblum and S. H. Gellman, *J. Am. Chem. Soc.*, 2013, **135**, 11748–11751.

53 Z. Amso and Z. Hayouka, *Chem. Commun.*, 2019, **55**, 2007–2014.

54 Y. H. Lau, P. de Andrade, Y. Wu and D. R. Spring, *Chem. Soc. Rev.*, 2014, **44**, 91–102.

55 D. P. Fairlie and A. D. de Araujo, *Peptide Sci.*, 2016, **106**, 843–852.

56 M. Moiola, M. G. Memeo and P. Quadrelli, *Molecules*, 2019, **24**, 3654.

57 X. Li, S. Chen, W.-D. Zhang and H.-G. Hu, *Chem. Rev.*, 2020, **120**, 10079–10144.

58 R. Gautier, D. Douguet, B. Antonny and G. Drin, *Bioinformatics*, 2008, **24**, 2101–2102.

59 N. Sreerama and R. W. Woody, *Anal. Biochem.*, 2000, **287**, 252–260.

60 M. J. Abraham, T. Murtola, R. Schulz, S. Páll, J. C. Smith, B. Hess and E. Lindahl, *SoftwareX*, 2015, **1–2**, 19–25.

© 2021 The Author(s). Published by the Royal Society of Chemistry

RSC Chem. Biol., 2021, **2**, 1608–1617 | **1617**